J. Fluid Mech. (2010), *vol.* 647, *pp.* 13–26.
doi:10.1017/S0022112009993600

Short-term forecasts and scaling of intense events in turbulence

D. A. DONZIS[1]† AND K. R. SREENIVASAN[2,3]

[1]Department of Aerospace Engineering, Texas A&M University, College Station, TX 77843, USA

[2]Institute for Physical Science and Technology, University of Maryland, College Park, MD 20742, USA

[3]Department of Physics and Courant Institute, New York University, NY 10012, USA

(Received 25 July 2009; revised 19 November 2009; accepted 20 November 2009)

Extreme events such as intense tornadoes and huge floods, though infrequent, are particularly important because of their disproportionate impact. Our ability to forecast them is poor at present. Large events occur also in intermittent features of turbulent flows. Some dynamical understanding of these features is possible because the governing equations are known and can be solved with good accuracy on a computer. Here, we study large-amplitude events of turbulent vorticity using results from direct numerical simulations of isotropic turbulence in conjunction with the vorticity evolution equation. We show that the advection is the dominant process by which an observer fixed to the laboratory frame perceives vorticity evolution on a short time scale and that the growth of squared vorticity during large excursions is quadratic in time when normalized appropriately. This result is not inconsistent with the multifractal description and is simpler for present purposes. Computational data show that the peak in the viscous term of the vorticity equation can act as a precursor for the upcoming peak of vorticity, forming a reasonable basis for forecasts on short time scales that can be estimated simply. This idea can be applied to other intermittent quantities and, possibly, more broadly to forecasting other extreme quantities, e.g. in seismology.

1. Introduction

Huge floods, intense tornadoes and hurricanes, large earthquakes, big crashes in stock-market value and a number of other extreme events have much larger impact than might be reckoned by the relatively low frequency of their occurrence. Forecasting such events is of obvious interest but of momentous challenge. By a forecast, we mean here the advance knowledge that a certain large event will occur with high probability within a known time scale following a suitable precursor. If successful predictions are possible in one complex system, something useful may be learnt about others as well.

Turbulence is replete with strong fluctuations in vorticity, dissipation and other features characteristic of small-scale motion. Depending on the Reynolds number, extreme fluctuations of dissipation and vorticity can be hundreds or thousands of times the mean value (Sreenivasan & Meneveau 1988; Donzis, Yeung & Sreenivasan 2008). It is technically important to understand these extremes because of their relevance to

† Email address for correspondence: donzis@tamu.edu

reacting flows (Sreenivasan 2004) and dispersion problems (Borgas & Yeung 2004); they are also objects of intense mathematical inquiry (Gibbon & Doering 2005) and the centre of attention in intermittency theories (Frisch 1995; Yakhot & Sreenivasan 2005). Our interest here is to explore empirically the extent to which extreme events in turbulence can be predicted dynamically through a plausible precursor. Such dynamical predictions are indeed difficult, but we have here the luxury of being able to learn from the well-posed differential equations governing fluid motion. Though the analytical understanding of the equations is modest, we expect to track their behaviour well through 'exact' numerical solutions. This is the thrust of the paper.

The numerical database for our work comes from the exact or direct numerical simulation (DNS) of isotropic turbulence. We have performed three such simulations at Taylor microscale Reynolds numbers R_λ of 140, 240 and 400 to obtain all the terms in the vorticity equation (Donzis *et al.* 2008). We use the data to study the processes that dominate the time variation of vorticity at a fixed location, and we identify precursors of extreme events in the vorticity trace. We find that advection dominates the dynamics for short times and that the Eulerian growth of extreme vorticity follows a universal power law with a single exponent when normalized by the proper time scale. Perhaps against intuition, strong viscous activity typically precedes intense vorticity, and the advance time is given by a suitable combination of viscosity and large-scale velocity. In particular, the knowledge of the signs of the advective and viscous terms, and of the vorticity itself, determines in advance the occurrence of a local extremum in vorticity.

The rest of the paper is organized as follows. We first describe the numerical simulations and the basic parameters that they employ. The dynamics of large fluctuations of vorticity are studied in the next two sections through the evolution equation. The time scales associated with large events are discussed, and precursors of large fluctuations are presented. Finally, a summary and further outlook are offered.

2. Numerical method and simulation parameters

Our interest is in the time evolution of vorticity ω_i, whose governing equation

$$\partial\omega_i/\partial t = -u_j\omega_{i,j} + \omega_j u_{i,j} + \nu\omega_{i,jj} \tag{2.1}$$

results from taking the curl of the Navier–Stokes equations for an incompressible fluid. Here, u_i represents the velocity component in the direction i and the summation notation is implied; ν is the kinematic viscosity of the fluid. The equation is solved using a massively parallel implementation of the pseudo-spectral method of Rogallo (1981). Aliasing control is applied by a combination of truncation and phase-shifting methods to compute all the terms in this equation, which implies double evaluations for the first two terms on the right. This adds significant overhead to the computational time. However, since large fluctuations occur on short time scales, statistics appear to converge without demands of excessively long simulations. Further, one can obtain a large number of samples by storing the data at many locations in physical space at every time step: homogeneity assures that specific locations are unimportant for statistics, as long as they are sufficiently distant from one another to be effectively independent.

The initial conditions are taken from stationary forced isotropic turbulence at the Reynolds numbers given in Table 1, and the resolution is such that the condition $k_{max}\eta \approx 1.5$ holds (where k_{max} is the highest resolvable wavenumber and η is the Kolmogorov scale representing, nominally, the smallest scale of dissipation). The

R_λ	140	240	400
N	256	512	1024
$T_{E,0}/\langle\tau_\eta\rangle_0$	14.5	23.7	40.8
$T_{E,0}/\langle\tau_v\rangle_0$	459	1310	4244
$\langle\tau_\eta\rangle_0/\langle\tau_v\rangle_0$	32	55	104

TABLE 1. Basic parameters of the simulations: Taylor microscale Reynolds number R_λ, grid resolution N and different time scale ratios at the beginning of the simulation (denoted by the subscript 0). Here, $T_{E,0} \equiv L/u_0'$ is the eddy turnover time, with L being the large scale of turbulence and u_0' the root-mean-square (r.m.s.) velocity; $\langle\tau_\eta\rangle_0 = (\nu/\langle\epsilon\rangle_0)^{1/2}$ is the Kolmogorov time scale; and $\langle\tau_v\rangle_0 = \nu/u_0'^2$ is a characteristic time scale of extreme events (see the text). Further, $\langle . \rangle$ indicates space average.

simulations were continued without forcing. Since the simulation time was short, the final value of turbulent kinetic energy was always greater than half its initial value, and the variation of the smallest time scale τ_η was less than 40 %.

The time step size was controlled by a constant Courant number of about 0.3 which is smaller than in common practice (Eswaran & Pope 1988). This resulted in a time step that is two orders of magnitude smaller than the mean Kolmogorov time scale. Indeed, faithful capture of the strongest events requires such a fine resolution.

3. Dynamics and statistics of large fluctuations

3.1. *Power-law behaviour*

To discuss the dynamics of large excursions in vorticity ω_i, it is convenient to rewrite (2.1) schematically as

$$\partial\omega_i/\partial t = -\mathscr{C}_i + \mathscr{W}_i + \mathscr{V}_i, \tag{3.1}$$

where

$$\mathscr{C}_i = u_j\omega_{i,j}, \quad \mathscr{W}_i = \omega_j u_{i,j} \quad \text{and} \quad \mathscr{V}_i = \nu\omega_{i,jj}, \tag{3.2}$$

representing the advective, vortex-stretching and viscous contributions, respectively. In figure 1 we show typical time series, for ω_1, of all the terms in (3.1). The figure shows that the advective term $\mathscr{C}_i$ accounts for much of the variation of ω_i, especially when the vorticity amplitudes are large. The Eulerian picture is that large excursions of vorticity, perhaps related to vortical structures, are advected by the local flow past the measuring location. This observation, which is consistent with the qualitative suggestions in Zeff *et al.* (2003) and Lee & Lee (2005), would imply that

$$\partial\omega_i/\partial t \approx -\mathscr{C}_i \tag{3.3}$$

can approximate the dynamics of large fluctuations of vorticity. Vortex stretching, which is the main mechanism for generating vorticity, makes a secondary contribution to the instantaneous balance of large fluctuations observed in figure 1. The physical picture is that large vorticity is generated on a longer time scale dictated mostly by vortex stretching and that once created, it is advected by the flow on shorter time scales. Let us denote the instantaneous advection velocity by v. Since viscous effects eventually prevent large spatial gradients from forming, it is natural to think that both ν and v are the two key variables for scaling the dynamics of large fluctuations.

Let us choose a vorticity spike such as that highlighted in figure 1. Since $\mathscr{C}_i$ dominates the right-hand side of (3.1), ω_i will have an inflection point at time t'

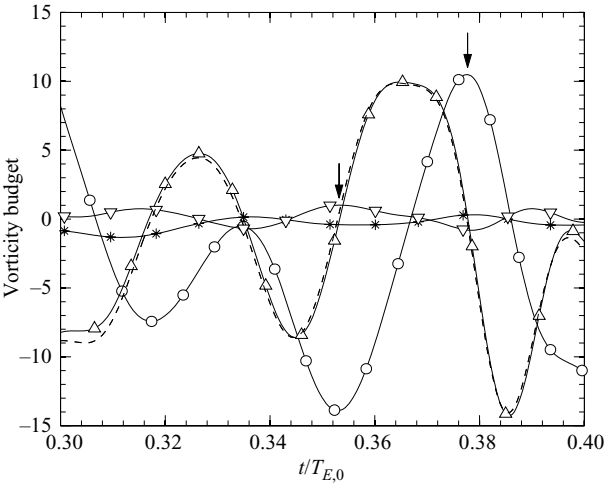

FIGURE 1. Typical time series for the vorticity budget in (3.1) at an arbitrary spatial location for $R_\lambda \approx 240$. All quantities are normalized by the r.m.s. value of ω_1 at $t = 0$ and by the initial eddy turnover time $T_{E,0} = L/u_0'$. Lines represent the data and symbols mark the lines for visibility. The dashed lines denote $\partial\omega_1/\partial t$; the upright triangles denote $-\mathscr{C}_1$; the stars denote $\mathscr{W}_1$; and the inverted triangles denote $\mathscr{V}_1$.The circles represent ω_1 multiplied by 10 for clarity. The arrows indicate typical maxima in ω_1 and $\mathscr{V}_1$.

where the advection term has a local maximum. One can expand the solution around t' which, to first order, is $\partial\omega_i/\partial t \approx c$, where the constant c, the local maximum of $\mathscr{C}_i$, is written as $1/\tau^2$ for convenience. Integration yields $\omega_i \approx \omega_i^0 + (t - t')/\tau^2$, where ω_i^0, the vorticity at t', is typically much smaller than the peak value. Therefore, one expects

$$\omega_i^2 \sim (t - t')^2/\tau^4 \tag{3.4}$$

during those intervals in which vorticity grows fast. The quality of this prediction is shown in figure 2 for a typical intense event at $R_\lambda \approx 400$. Equation (3.4) is seen to represent the data quite well for more than an order of magnitude in the fluctuation amplitude; this is so for all large peaks.

To test (3.4) further, we have obtained least squares fits of the expression

$$\omega_i^2 = [\alpha_1(t - t')]^{\alpha_2} \tag{3.5}$$

to intense events at different Reynolds numbers. The resulting α_2 values are plotted in figure 3 against the parameter $\theta = (\nu\overline{\epsilon})^{1/2}/\overline{v}^2$, with the overbar denoting the average over the duration of the peak vorticity. To be specific, we have used the averaging time to be the interval between the circles in figure 2, but plausible variants do not affect the results significantly. The origin and interpretation of the parameter θ will be discussed in a moment. The inset of figure 3 plots the same exponent α_2 as a function of the maximum value of vorticity attained in each intense event examined. It appears that $\alpha_2 = 2$ holds essentially for fluctuations of all intensities (which span almost three decades here; see the inset) and for all R_λ.

In the multifractal (MF) formalism, different magnitudes of squared vorticity have different exponents (Sreenivasan & Meneveau 1988), but (3.4) and the data presented here yield a unique exponent of 2 for all large magnitudes. The two views are, in fact, consistent if we note that τ in (3.4) depends on the intensity of each peak and

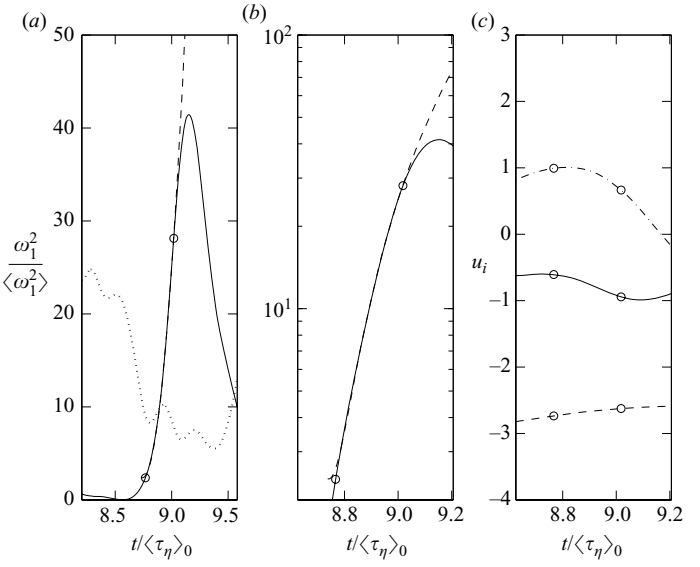

FIGURE 2. Detailed view of a typical intense event at $R_\lambda \approx 400$. (*a*) Squared vorticity normalized by its space average at the beginning of the simulation. The dotted line corresponds to $10\epsilon/\langle\epsilon\rangle_0$ (where ϵ is the instantaneous energy dissipation rate; see § 3.2 for definition) at the same location; the factor 10 has been used for clarity. (*b*) Squared vorticity on semi-log scale. (*c*) Velocity components during the same time interval considered in (*a*) and (*b*). The relevance of these data will be discussed in § 3.2. Times are normalized by the initial space-averaged Kolmogorov time scale $\langle\tau_\eta\rangle_0$. The dashed lines in (*a*) and (*b*) correspond to best fits using (3.4), and the circles delimit the fitting range.

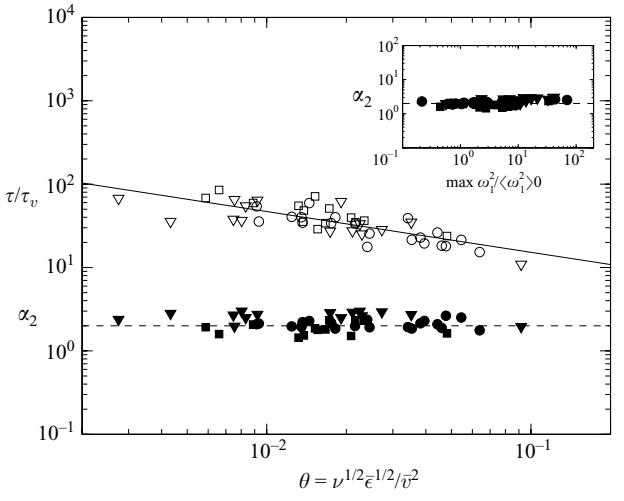

FIGURE 3. The filled symbols denote the exponent α_2 in (3.5). The dashed line at magnitude 2 is for comparison. The unfilled symbols denote normalized time scale τ/τ_v in (3.4). The circles, squares and triangles correspond to data at $R_\lambda \approx 140$, 240 and 400, respectively. The solid line is for $\tau/\tau_v \sim \theta^{-0.49}$. The inset shows the exponent α_2 as a function of the peak value of the corresponding large event.

effectively hides the circumstance of variable exponents. A fuller discussion of this point is given in the Appendix.

3.2. *Time scales*

Figure 3 also shows the similarity scaling of τ (which, through (3.4), is readily related to α_1 in (3.5)). To understand its nature, recall the earlier remark that ν and the advection velocity v are two key parameters. It is reasonable to choose the average velocity $\overline{v}$, over the duration of the event, as the appropriate characteristic value, but the precise choice is not critical: it is clear from figure 2 that even when the vorticity varies by orders of magnitude, the velocity remains approximately constant (figure 2*c*). This is consistent with the well-known fact that vorticity and velocity gradients vary on shorter time scales than the velocity itself. We now note that $c = -u_j\omega_{i,j}$ (see (3.3)) and that $\boldsymbol{\varepsilon}_{ijk}u_i\omega_{k,j} = \epsilon/\nu - 2(u_i s_{ij})_{,j}$, where $\boldsymbol{\varepsilon}_{ijk}$ is the alternating tensor and ϵ is the energy dissipation rate. The second relation shows that cross-terms involving components of the velocity and vorticity gradients are kinematically related in part to instantaneous dissipation. Moreover, it has been consistently found that intense enstrophy events are 'preceded' by intense dissipation events (Zeff *et al.* 2003; Lee & Lee 2005). Therefore, in view of (3.3), it is reasonable to think that ϵ is also a key parameter in determining the dynamics close to an intense vortical event. Unlike the velocity, the dissipation over the duration of an intense vorticity episode varies substantially, as can be seen in figure 2(*a*); so it is necessary to consider its average value $\overline{\epsilon}$. Two time scales, $\tau_v = \nu/\overline{v}^2$ and $\tau_\eta = (\nu/\overline{\epsilon})^{1/2}$, can then be formed from ν, $\overline{v}$ and $\overline{\epsilon}$. The ratio of these two time scales is the non-dimensional parameter $\theta = (\nu\overline{\epsilon})^{1/2}/\overline{v}^2$. Dimensional analysis suggests that

$$\tau = \tau_v f(\theta), \tag{3.6}$$

where f should be some universal function. This is the expectation explored in figure 3 over (almost) two orders of magnitude of θ.

The DNS results at different Reynolds numbers are included in figure 3 (open symbols). Some scatter notwithstanding, the data in figure 3 support the scaling suggested by (3.6) and can be fitted to the expression $\tau/\tau_v \sim \theta^{-\gamma_\theta}$ with $\gamma_\theta \approx 0.49$. The results do not change qualitatively if θ and τ are defined through other plausible averaging times. Note that the magnitude of τ_v varies by an order of magnitude in our study, as can be seen from Table 1, where its 'global' mean-square velocity u'^2 is used instead of $\overline{v}^2$. This substitution does not mask this order of magnitude statement.

Each intense event is slightly different from all others, since (3.3) is only an approximation that depends on the relative weights of advection, vortex stretching and dissipation; the levels of $\mathscr{W}_i$ and $\mathscr{V}_i$ would, in fact, be different in the neighbourhood of different spikes, giving somewhat different values of the constant c. Nevertheless, the DNS data follow the simple correlation with constant α_2. In principle, it would be possible to account for fluctuations of $\mathscr{W}_i$ and $\mathscr{V}_i$ as random variables on the right-hand side of (3.3), which could lead to an additive noise to τ in (3.6). The distribution of τ is related to the scatter in figure 3, which itself is related to how vortex-stretching and viscous contributions are crudely eliminated from inclusion. This effect, however, would weaken with increasing Reynolds numbers because the intense events and advection effects would both become stronger.

We emphasize that the scaling $\omega_i^2 \sim t^2$ is simply a first-order expansion around the local maximum of $\partial\omega_i/\partial t$. This general observation applies to any function. What is particular to turbulence is that the time scale associated with this growth can be related to a simple combination of parameters. This is mainly because a single

process dominates the right-hand side of (3.1). If, for instance, advection grows in time negatively but viscous terms attain large values to balance advection, the proper time scale for the growth of ω_i will be more complex.

A further point is in order. From (3.6) it may appear that intense vorticity events are completely determined by local conditions. One has to reconcile it with the global organization observed in turbulent flows. Our derivations for the behaviour of ω_i contain the velocity $\boldsymbol{u}$ and the dissipation rate ϵ. In terms of vorticity, the velocity field can be written as $\boldsymbol{u}(\boldsymbol{x}) = -1/4\pi \int_\Lambda \boldsymbol{\omega}(\boldsymbol{x}-\boldsymbol{r}) \times \boldsymbol{r}/|\boldsymbol{r}|^3 \mathrm{d}^3\boldsymbol{r}$, where Λ is the periodic domain. This equation makes it clear that the velocity at a particular location contains information from vorticity everywhere, especially from a neighbourhood of $\boldsymbol{x}$ (because of the factor $\boldsymbol{r}/|\boldsymbol{r}|^3$). A similar integral relation can be obtained for velocity gradients and thus for ϵ (see, e.g. Constantin 1994). Therefore, (3.4) and (3.6) do not mean that only local information is adequate to addressing the scaling of intense vortical events.

4. Precursors of large fluctuations

4.1. *Precursors in viscous term*

The results in the previous section show that large fluctuations are approximated well by (3.3). Therefore, large values of $\mathscr{C}_i$ lead to large time derivatives which will result in the t^2 growth of squared vorticity. Of course, because of the integral relation between $\mathscr{C}_i$ and ω_i, there will be a time lag between a large value of advective terms and a peak in ω_i. This is clearly seen in figure 1 where peaks in ω_i (the line connecting the circles) appear later than the peaks in $\mathscr{C}_i$ (the line connecting the upright triangles). Furthermore, large advective terms are preceded by local maxima of viscous terms (the line connecting the inverted triangles in figure 1). This feature can be understood if one writes the viscous term as $\mathscr{V}_i = \nu(\partial/\partial x_j)(\partial\omega_i/\partial x_j)$ and replaces $\partial/\partial x_j$ by $(1/\overline{v})\partial/\partial t$. This leads to $\mathscr{V}_i \approx (\nu/\overline{v})(\partial/\partial t)(\partial\omega_i/\partial x_j)$ which, to a first approximation, can be written from definitions (3.2) as $\partial\omega_i/\partial x_j \approx \mathscr{C}_i/\overline{v}$ within the short interval in which vorticity peaks, so that

$$\frac{\partial \mathscr{C}_i}{\partial t} \approx \frac{1}{\tau_v}\mathscr{V}_i. \tag{4.1}$$

Equation (4.1) furthermore shows that τ_v is the natural time scale of the problem. Indeed, if one assumes that $\mathscr{V}_i$ is represented by a single Fourier mode with frequency ϖ and amplitude $\hat{\mathscr{V}}_i$, (3.3) and (4.1) suggest that $\mathscr{V}_i$ arrives at an observation point earlier than ω_i by the time interval of $2\pi\tau_v/\varpi$. In other words, the time interval Δt^* between the local maxima for $\mathscr{V}_i$ and ω_i (illustrated in figure 1 as the interval between the arrows on the curves for ω_1 and $\mathscr{V}_1$) is of the form

$$\Delta t^* \sim \tau_v. \tag{4.2}$$

We automate the search for scaling of (4.2) by first focusing attention on values of ω_1^2 greater than, say, 30 times the mean-square value for the time series obtained at one spatial location. Then, for each such peak, a prior local maximum of $\mathscr{V}_i$ is identified within an interval corresponding to a few mean values of τ_v. Experience shows that the precise choice of this interval is not critical for the scaling to be determined. This simple approach, however, does miss some spikes: in the chosen interval, there may be more than one maximum for $\mathscr{V}_i$ or more than one ω_i above the specified threshold. The data presented here capture the conditions properly for about 75 % of the samples above the threshold. We measure the time Δt^* between the local maxima for $\mathscr{V}_i$ and ω_i and empirically test (4.2) by also measuring τ_v independently.

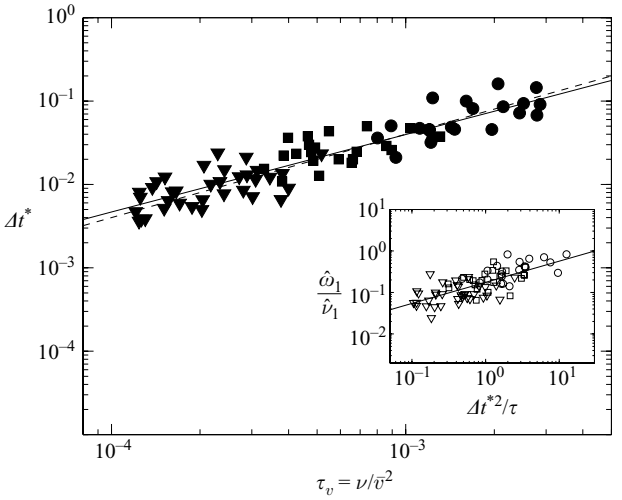

FIGURE 4. The time interval Δt^* between the arrivals of a peak in viscous terms and the subsequent peak in vorticity plotted against the time scale τ_v for $R_\lambda \approx 140$ (circles), 240 (squares) and 400 (triangles). The dashed line denotes slope 1. The solid line denotes (4.3) which is the best fit to the data. The inset denotes scaling of the ratio of local maxima for vorticity $\hat{\omega}_1$ and viscous terms $\hat{\mathscr{V}}_1$.

To capture the dynamics over the interval between local maxima of $\mathscr{V}_i$ and ω_i, it is more convenient to average the velocity v over the time interval Δt^*; the results to be discussed below are robust with respect to the use of this longer averaging time, since as seen in figure 2, the velocity does not vary significantly over such intervals of time. In figure 4 we see that the data for $R_\lambda \approx 140$, 240 and 400 follow

$$\Delta t^* \approx 24 \tau_v^{0.93}, \tag{4.3}$$

which is only slightly different from (4.2). The agreement in figure 4 is good especially because this scaling is not of statistical nature but corresponds to individual trajectories in phase space. It is the case, regrettably, that the present argument lacks the connection to geometrical aspects of the vectors and tensors involved. In particular, the model does not consider the effect of alignments between the velocity vector $\boldsymbol{u}$ and the gradient $\nabla\omega_1$ which make up the advective term (i.e. $\mathscr{C}_1 = \boldsymbol{u} \cdot \nabla\omega_1 = |\boldsymbol{u}||\nabla\omega_1| \cos(\boldsymbol{u}, \nabla\omega_1)$). These aspects can be taken into account at the next level of refinement, presumably reducing the scatter in figure 4, but the dimensionality of the problem will increase disproportionately. Finally, as stressed in previous sections, (3.3) contains in reality some contribution from $\mathscr{V}_i$ and $\mathscr{W}_i$, which may be different for each intense event. In this sense, the scaling (4.3) can be regarded as an approximate and average result.

To get some idea of the relation between the amplitude of ω_i and $\mathscr{V}_i$, we may again resort to a single Fourier component for the viscous term with amplitude $\hat{\mathscr{V}}_i$. Equations (3.3) and (4.1) then imply $\hat{\omega}_1/\hat{\mathscr{V}}_1 \sim \tau_v/\varpi^2$. Now, we use the previous result $\Delta t^* \sim \tau_v/\varpi$ to find that the amplitude ratio scales as $\hat{\omega}_1/\hat{\mathscr{V}}_1 \sim \Delta t^* 2/\tau_v$. To compare this prediction with the DNS results, the vorticity 'amplitude' is taken as the difference between the maximum value and that at the time when $\mathscr{V}_i$ peaks; this difference measures the actual growth. The results are shown in figure 4 (inset) where the data follow the power-law trend, although the slope is smaller than the expected value of

R_λ	140	240	400
$N_{\hat{\mathscr{V}}_i}$	190	198	155
$P(\hat{\omega}_i \vert \hat{\mathscr{V}}_i)$	0.71	0.71	0.72
$P(\mathrm{sign}(\hat{\omega}_i) = \mathrm{sign}(\hat{\mathscr{V}}_i) \vert \hat{\mathscr{V}}_i)$	0.48	0.45	0.50
$P(\mathrm{sign}(\hat{\omega}_i) = \mathrm{sign}(\hat{\mathscr{V}}_i) \vert \hat{\mathscr{V}}_i, (+++/---))$	1.00	1.00	1.00
$P(\mathrm{sign}(\hat{\omega}_i) = \mathrm{sign}(\hat{\mathscr{V}}_i) \vert \hat{\mathscr{V}}_i, (+-+/-+-))$	0.82	1.00	0.77
$P(\mathrm{sign}(\hat{\omega}_i) = \mathrm{sign}(\hat{\mathscr{V}}_i) \vert \hat{\mathscr{V}}_i, (++-/--+))$	0.88	0.78	0.80
$P(\mathrm{sign}(\hat{\omega}_i) = \mathrm{sign}(\hat{\mathscr{V}}_i) \vert \hat{\mathscr{V}}_i, (+--/-++))$	0.46	0.40	0.50

TABLE 2. Intense viscous event as a precursor for the subsequent large vorticity event. The threshold for $\mathscr{V}_i$ is $\langle \omega_1^2 \rangle_0$. See the text for explanations of different quantities.

unity (0.53 from the best fit). This result and the greater scatter than in the main frame in figure 4 are not unexpected because although τ_v is the natural time scale for the problem, the dimensional scaling for the ratio of amplitudes relies on $\mathscr{V}_i$ behaving as a single sinusoid.

4.2. *Prediction results*

The scaling of (4.3) shown in figure 4 was obtained by analysing time series backwards: how far back in time with respect to an intense vorticity event does a local extremum in $\mathscr{V}_i$ occur? We can now ask the more important question of forecast: using the correlations just described, how long after observing a local maximum in the viscous event does it take for intense vorticity to build up to its peak value? We first note that large $\mathscr{C}_i$ will not always lead to large ω_i. An example is seen in figure 1 at $t/T_{E,0} \approx 0.326$, where $\mathscr{C}_i$ attains a large value but ω_i is negative for a long interval of time. Thus, the large positive time derivative is not enough by itself to make ω_i grow to large positive values.

We now proceed to explain the last statement better and answer the question posed above. This is not altogether a circuitous exercise because there are several operational considerations in the prediction task than are involved in data correlation. First, we find the local maximum (or minimum) in $\mathscr{V}_i$ if it is positive (or negative). Since we are primarily interested in large fluctuations, we simultaneously set a threshold on $\mathscr{V}_i$. Let us denote a qualified maximum (or minimum) by $\hat{\mathscr{V}}_i$ and the time at which it occurs by $t_{\hat{\mathscr{V}}_i}$, and let the total number of such viscous events, both positive and negative, observed for a given Reynolds number be $N_{\hat{\mathscr{V}}_i}$. We now look for a local extremum for ω_i in an interval of time given by $2 \times 24\tau^{0.93}$ (see (4.3)), where the prefactor 2 roughly accounts for the scatter observed in figure 4. If a local extremum exists, we increment $N_{\hat{\omega}_i}$, the total number of extrema for ω_i following an intense viscous event. In table 2 we show $N_{\hat{\mathscr{V}}_i}$ and $P(\hat{\omega}_i \vert \hat{\mathscr{V}}_i)$, the probability of finding a local extremum of ω_i knowing that there was an intense viscous event (i.e. the ratio $N_{\hat{\omega}_i}/N_{\hat{\mathscr{V}}_i}$), for different Reynolds numbers using a threshold for $\mathscr{V}_i$ equal to $\langle \omega_1^2 \rangle_0$. The table (third row) shows that slightly more than 70 % of intense viscous events are followed by the maxima in vorticity in the interval given by (4.3) for all R_λ. Thus, 70 % of the events can be forecast in time scales of the order τ_v. The results could not be much better because our procedure for tracking sequential peaks in the viscous and vorticity terms was successful only 75 % of the time. Note further that this result comprises local extrema for ω_i of both signs. On the other hand, the probability with which a positive or negative sign of large $\mathscr{V}_i$ would lead to a large positive or

negative sign of ω_i is close to 50 % (fourth row of table 2) – an essentially random connection.

It is possible to use additional information about the state of the system at $t_{\hat{\mathscr{V}}_i}$ to successfully predict more often the occurrence of a vorticity event knowing that a strong viscosity event has occurred. To do this, we distinguish different cases on the basis of the signs of $\mathscr{V}_i$, $-\mathscr{C}_i$ and ω_i at $t = t_{\hat{\mathscr{V}}_i}$. A state of the system will be denoted by $(+++)$ if $\mathrm{sign}(\mathscr{V}_i(t_{\hat{\mathscr{V}}_i})) = 1$, $\mathrm{sign}(-\mathscr{C}_i(t_{\hat{\mathscr{V}}_i})) = 1$ and $\mathrm{sign}(\omega_i(t_{\hat{\mathscr{V}}_i})) = 1$ or $(+--)$ if $\mathrm{sign}(\mathscr{V}_i(t_{\hat{\mathscr{V}}_i})) = 1$, $\mathrm{sign}(-\mathscr{C}_i(t_{\hat{\mathscr{V}}_i})) = -1$ and $\mathrm{sign}(\omega_i(t_{\hat{\mathscr{V}}_i})) = -1$. Now we look at the probability of finding an extreme $\hat{\omega}_i$ given that there was an intense viscous event $\hat{\mathscr{V}}_i$ and that the configuration is given by $(+++)$. Other combinations can be defined similarly. Note that $(+++)$ and $(---)$ are equivalent, as are $(+-+)$ and $(-+-)$. The equivalent states are collected together in table 2. We see that when $\mathscr{V}_i$, $-\mathscr{C}_i$ and ω_i all have the same sign (i.e. $(+++)$ or $(---)$), an intense viscous event always results in a local extremum for ω_i of the same sign, with the intensity that may be related to the scaling shown in the inset of figure 4. If either $-\mathscr{C}_i(t_{\hat{\mathscr{V}}_i})$ or $\omega_i(t_{\hat{\mathscr{V}}_i})$ has a different sign, the probability is reduced as expected – to about 80 % at all Reynolds numbers.

Thus, we find that the viscous term $\mathscr{V}_i$ is a reasonable precursor (with 70 % success) for intense vorticity events on time scales of the order of τ_v. One can do better in several ways. For example, if this information is supplemented by the sign of the advective term and vorticity itself at the instant $\mathscr{V}_i$ peaks, the precursor becomes more definitive (almost always successful for one set of conditions and about 80 % successful for others). Although the conditional probabilities shown in Table 2 appear to be independent of the Reynolds number, longer time series and a wider range of Reynolds numbers are needed to strengthen this assertion.

5. Discussion and conclusions

We have shown that large viscous contributions anticipate the arrival of large vorticity events. This statement can be understood as follows. Since advection dominates, gradients in space and time are related by a velocity. Therefore, gradients of vorticity gradients (i.e. viscous terms) may be treated as time derivatives of vorticity gradients and therefore may 'announce' the arrival of the large vorticity gradients or, for quasi-constant velocity, large advective terms. The structure of the fluid dynamic equations makes viscous terms (under the dominance of advection) 'look like' the second time derivative of vorticity and is capable of anticipating the arrival of large vorticity. This anticipation cannot be expected to hold true for long periods.

All intermittent quantities of turbulence (such as dissipation) are governed by equations with a structure similar to (3.1), with the 'sources' $\mathscr{W}_i$ and $\mathscr{V}_i$ replaced suitably. Whenever the contributions from all these processes are small compared with $\mathscr{C}_i$ for intense events, (3.3) applies qualitatively. Therefore, it is possible that the scaling laws proposed here may hold qualitatively for all intermittent quantities. The physical picture would be that they would all be advected by the flow on short time scales, but different processes would be responsible for building up the large fluctuations on longer time scales.

While our results do not depend significantly on averaging times and procedures, there are at least two limitations to our proposal on precursors. First, 'predictions' are possible on relatively short time scales of the order of some 20 τ_v; the time scale τ_v is of the order of the Kolmogorov time in box turbulence and will be multiplied by a factor $U/\overline{v}$ if vorticity advection occurs by a mean velocity U instead of the

fluctuation. It is unclear if forecasts over longer times would be possible in practice (without a more elaborate apparatus). Second, it is not obvious that one can measure the second derivative of the signal with adequate accuracy. It presents no problem in a clean system such as computational turbulence, but in general, one has to apply some filtering to the signal without losing its substance.

We note that the work presented here has been mainly from a Eulerian perspective. Lagrangian studies following specific structures will be of great fundamental value. These studies are, in fact, part of our continuing work.

Although we do not have the luxury of well-tested differential equations for many extreme events occurring in nature, we believe that knowledge from turbulence could prove valuable for them as well. It has already been observed in Donzis *et al.* (2008), and theorized, among others, in L'vov & Procaccia (1996), Nelkin (1999) and He *et al.* (1998), that universal behaviour may govern aspects of all extreme phenomena. In seismology, for instance, there is some evidence for the existence of precursory motion for earthquakes and aftershocks (see, for example, Melbourne & Webb 2002). In particular, measured displacement shows departures from long-term trends which will first be captured by changes in second time derivatives. It is conceivable that this precursor is related to shear stresses (and therefore to dissipation). Even for non-Newtonian fluids, dissipative contributions are determined by velocity gradients through a (sometimes-complex) functional form. The corresponding term in the momentum equation would then take the form of the gradient of this function. In this case too, strong dissipative terms may serve as a precursor for intense events if space and time can be related (as shown to be the case for vorticity events). Some of the fluid dynamics involved in such problems has been discussed in e.g. Shimamoto (1986) and Rice (2006). A more rigorous relation between fault dynamics and fluid mechanics is part of our ongoing research.

It is a pleasure to dedicate this paper to Professor S. H. Davis who, through personal research, leadership and mentoring, has immensely influenced the fluid dynamics community of his times. We appreciate helpful collaboration with P. K. Yeung on the simulations. This work was supported by the National Science Foundation grant CTS-0553602 to the University of Maryland.

Appendix. Relation to multifractal predictions

Here, we explore the connection between the present model of large fluctuations with other descriptions in the literature. Since (3.4) represents large fluctuations one would expect that a model based on this functional form should be able to reproduce high-order statistics from experimental and numerical data as well as the widely used MF models (Yakhot & Sreenivasan 2005). One can use a collection of power-law events of the form

$$\tilde{\omega}_1^2(t) \approx \begin{cases} [(t - t_{0-})/\tilde{\tau}]^{\beta}/\tilde{\tau}^2, & t_{0-} \leqslant t < t_p, \\ [(t_{0+} - t)/\tilde{\tau}]^{\beta}/\tilde{\tau}^2, & t_p \leqslant t < t_{0+}, \end{cases} \tag{A 1}$$

and zero otherwise, where t_p is the time at which $\tilde{\omega}_1^2$ attains its maximum, a, $t_{0\pm} = t_p \pm \delta t$ and $\delta t = \tilde{\tau}(\tilde{\tau}^2 a)^{1/\beta}$ so that $\tilde{\omega}_1^2(t_p) = a$. In this case, upon integration over time, one obtains moments that scale as

$$\langle \tilde{\omega}_1^{2n} \rangle \sim 2a^{1/\beta}\tilde{\tau}^{1+2/\beta}\frac{a^n}{1+\beta n}. \tag{A 2}$$

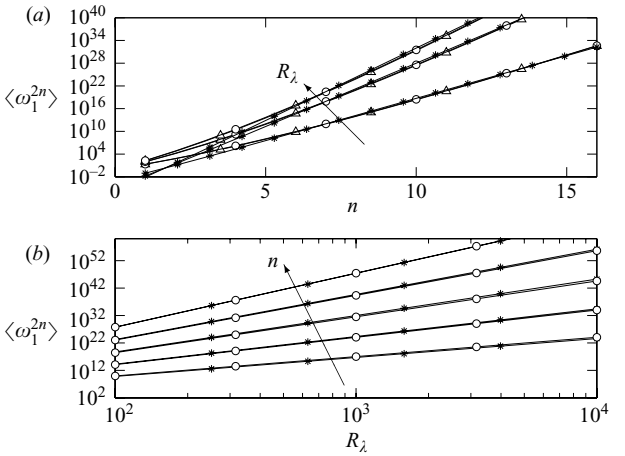

FIGURE 5. Scaling of moments according to MF (Nelkin 1990) (○), the theory of Yakhot & Sreenivasan (2005) (△) and (A 2) with effective parameters a^* and $\tilde{\tau}$ (∗). (*a*) The curves are for $R_\lambda = 100$, 500 and 1000. (*b*) Even moments from $n = 6$ to $n = 14$.

We have tested this scaling for signals with a number of spikes with different amplitudes a and times scales $\tilde{\tau}$ and found that (A 2) is quite accurate if one uses 'effective' parameters a^* and $\tilde{\tau}^*$ to fit the data. In figure 5(*a*), we show moments of squared vorticity according to the MF formalism (Nelkin 1990), the theory in Yakhot & Sreenivasan (2005) and (A 2) with parameters a^* and $\tilde{\tau}^*$ chosen as best fit to the MF model for $n \geqslant 5$ at three Reynolds numbers. As with some other models (Nelkin 1995; Schumacher, Sreenivasan & Yakhot 2007), it is virtually impossible to distinguish our model from the others from such comparisons alone. The matter is somewhat more obscure: by using 'exponential' spikes defined by $a\mathrm{e}^{c(t-t_p)}$ if $t \leqslant t_p$ and $a\mathrm{e}^{-c(t-t_p)}$ if $t > t_p$, one obtains $\langle\tilde{\omega}_1^{2n}\rangle \sim a^n/(nc)$ which is the same scaling as (A 2) for large n. Because the MF model, the power law (for any β) and the exponential spikes all give the same scaling for high-order moments, the conclusion is that little can be said about the local structure of intense events from such global comparisons.

Nevertheless, it is of interest to explore the connection between the present and the MF models. The fundamental assumption behind the latter is that the total dissipation in a d-dimensional box of size r scales as $E_r = \int_r \epsilon \, \mathrm{d}r \sim r^{\alpha-1+d}$ (a similar quantity can be defined for enstrophy as $W_r = \int_r \omega^2 \, \mathrm{d}r \sim r^{\alpha'-1+d}$). In Meneveau & Sreenivasan (1987) this scaling was tested for the dissipation surrogate $(\partial u/\partial t)^2$ for ϵ by plotting E_r as a function of r. One of their figures is reproduced here in figure 6(*b*) along with the approximate power law (dashed line) suggested by those authors. In figure 6(*a*), we show the scaling of the integral $(\tilde{W}_1)_t = \int_0^t \tilde{\omega}_1^2 \, \mathrm{d}t$ where $\tilde{\omega}_1^2$ is composed of six spikes of the form of (A 1) with different t_p and amplitudes a. Comparison of figures 6(*a*) and 6(*b*) reveals the same approximate power-law behaviour. It is therefore not surprising that similar predictions are found for the scaling of moments.

Because one of the effective parameters, a^*, is a measure of the strongest fluctuations, it is of interest to investigate its Reynolds number scaling. We found that the present model reproduces the MF predictions if one uses simple power laws $a^* \sim R_\lambda^{\gamma_a}$, $\tilde{\tau}^* \sim R_\lambda^{\gamma_\tau}$ and $M \sim R_\lambda^{\gamma_M}$ (where M is the number of spikes) with $\gamma_a \approx 1.60$, $\gamma_\tau \approx -0.84$ and $\gamma_M \approx 1.75$. Using this result, we can determine the Reynolds number scaling of

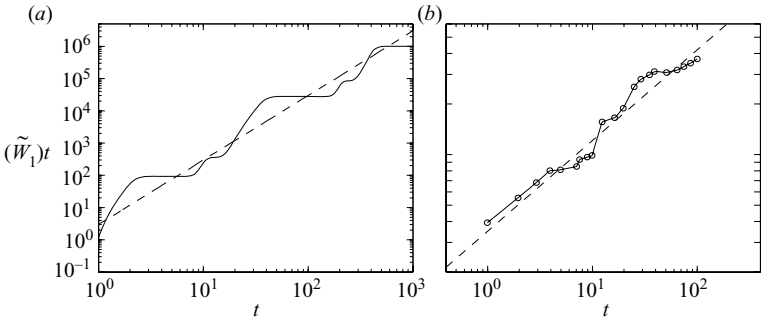

FIGURE 6. (*a*) The integral $(\tilde{W}_1)_t = \int_0^t \tilde{\omega}_1^2 \, \mathrm{d}t'$ for a signal composed of six spikes of the form of (A 1). The dashed line is a power law for comparison. (*b*) Experimental data from Meneveau & Sreenivasan (1987, figure 1*c* in their paper). The dashed line is the power-law fit from that reference. The two figures are in arbitrary units.

moments of different orders as

$$\langle \tilde{\omega}_1^{2n} \rangle \sim R_\lambda^{\,n\gamma_a + \rho - \log n / \log R_\lambda}, \tag{A 3}$$

where $\rho = \gamma_a/\beta + \gamma_\tau(1 + 2/\beta) - \gamma_M$. This equation shows a logarithmic correction to a simple power law at finite Reynolds numbers.

Another way to recast the MF model is to use local averages: $\epsilon_r/\langle\epsilon\rangle \sim (r/L)^{\alpha-1}$ for energy dissipation or $\omega_r^2/\langle\omega^2\rangle \sim (r/L)^{\alpha'-1}$ for squared vorticity. We are now interested in the limit $r \to 0$, so that r lies within an intense event. In the present model, we could write $\omega_r^2/\langle\omega^2\rangle \sim (r/r_\tau)^2$ (see (3.4)), where r_τ is a suitably defined scale (e.g. $r_\tau \approx v\,\tau$, this being a function of time and space). This result suggests a simpler object if scales are normalized by r_τ instead of L. In fact, we could write, at each location, $r_\tau^2\omega_r^2 \sim \langle\omega^2\rangle r^2$ and compute moments to obtain $\langle (r_\tau^2\omega_r^2)^n \rangle \sim \langle\omega^2\rangle^n r^{2n}$ (for $r \to 0$). This result, which can also be applied to ϵ, can be deduced from applying dimensional arguments to $r_\tau^2\epsilon_r$ – by assuming that the important parameters are $\langle\epsilon\rangle$ and r – resulting in non-anomalous scaling for the quantity $\langle (r_\tau^2\omega_r^2)^n \rangle$.

REFERENCES

BORGAS, M. S. & YEUNG, P. K. 2004 Relative dispersion in isotropic turbulence. Part 2. A new stochastic model with Reynolds-number dependence. *J. Fluid Mech.* **503**, 125–160.

CONSTANTIN, P. 1994 Geometric statistics in turbulence. *SIAM Rev.* **36**, 73–98.

DONZIS, D. A., YEUNG, P. K. & SREENIVASAN, K. R. 2008 Dissipation and enstrophy in isotropic turbulence: scaling and resolution effects in direct numerical simulations. *Phys. Fluids* **20**, 045108.

ESWARAN, V. & POPE, S. B. 1988 An examination of forcing in direct numerical simulations of turbulence. *Comp. Fluids* **16**, 257–278.

FRISCH, U. 1995 *Turbulence*. Cambridge University Press.

GIBBON, J. D. & DOERING, C. R. 2005 Intermittency and regularity issues in 3d Navier–Stokes turbulence. *Arch. Rat. Mech. Anal.* **177** (1), 115–150.

HE, G., CHEN, S., KRAICHNAN, R. H., ZHANG, R. & ZHOU, Y. 1998 Statistics of dissipation and enstrophy induced by localized vortices. *Phys. Rev. Lett.* **81**, 4636–4639.

LEE, S. & LEE, C. 2005 Intermittency of acceleration in isotropic turbulence. *Phys. Rev.* E **71**, 056310.

L'VOV, V. & PROCACCIA, I. 1996 The universal scaling exponents of anisotropy in turbulence and their measurements. *Phys. Fluids* **8**, 2565–2567.

MELBOURNE, T. I. & WEBB, F. H. 2002 Precursory transient slip during the 2001 $M_w = 8.4$ Peru earthquake sequence from continuous GPS. *Geophys. Res. Lett.* **29** (21), 2032.

Meneveau, C. & Sreenivasan, K. R. 1987 The multifractal spectrum of the dissipation field in turbulent flows. *Nucl. Phys.* B **2**, 49–76.

Nelkin, M. 1990 Multifractal scaling of velocity derivatives in turbulence. *Phys. Rev.* A **42** (12), 7226–7229.

Nelkin, M. 1995 Inertial range scaling of intense events in turbulence. *Phys. Rev.* E **52** (5), R4610–R4611.

Nelkin, M. 1999 Enstrophy and dissipation must have the same scaling exponents in the high Reynolds number limit of fluid turbulence. *Phys. Fluids* **11**, 2202–2204.

Rice, J. R. 2006 Heating and weakening of faults during earthquake slip. *J. Geophys. Res.* **111**, B05311.

Rogallo, R. S. 1981 Numerical experiments in homogeneous turbulence. NASA *Tech Rep*. 81315.

Schumacher, J., Sreenivasan, K. R. & Yakhot, V. 2007 Asymptotic exponents from low-Reynolds-number flows. *New J. Phys.* **9**, 89.

Shimamoto, T. 1986 Transition between frictional slip and ductile flow for halite shear zones at room temperature. *Science* **231**, 711–714.

Sreenivasan, K. R. 2004 Possible effects of small-scale intermittency in turbulent reacting flows. *Flow Turbul. Combust*. **72**, 115–131.

Sreenivasan, K. R. & Meneveau, C. 1988 Singularities of the equations of fluid motion. *Phys. Rev.* A **38**, 6287–6295.

Yakhot, V. & Sreenivasan, K. R. 2005 Anomalous scaling of structure functions and dynamic constraints on turbulence simulations. *J. Stat. Phys.* **121**, 823–841.

Zeff, B. W., Lanterman, D. D., McAllister, R., Roy, R., Kostelich, E. J. & Lathrop, D. P. 2003 Measuring intense rotation and dissipation in turbulent flows. *Nature* **421**, 146–149.